Journal of Thermal Biology 84 (2019) 323–330

Contents lists available at ScienceDirect

Journal of Thermal Biology

journal homepage: www.elsevier.com/locate/jtherbio

Numerical simulation of heat induced flow-mediated dilation of blood vessels

Yabo Wang[a,*], Kai Zhu[a], Jinshan Wang[a], Long Yang[b]

[a] Tianjin Key Laboratory of Refrigeration Technology, Tianjin University of Commerce, Tianjin, China
[b] Tianjin First Central Hospital, Tianjin, 300192, China

ARTICLE INFO

Keywords:
Local heat
Blood flow
Flow mediated
Dilation

ABSTRACT

Local heat can accelerate the blood circulation and induce the vasodilatation. Investigators reported that local heat causes an increase in skin blood flow consisting of two phases. The first is solely sensory neural, and the second is nitric oxide mediated. However, the mechanism underlying the skin blood flow response to local heating are complex and poorly understood. The mechanisms behind these two phases are deduced to be linked by flow-mediated dilation. In this study, the variation of the blood flow and the blood vessel diameter are monitored during local heating. According to the dynamic blood flow, the theoretical model of flow mediated dilation involving the key agents production and transportation was first used to study vasodilatation process during heating, and the variations of blood vessel was obtained. Finally, accurate distributions of the nitric oxide, calcium and myosin concentrations in the arterial wall were found during autoregulation. We evaluated the time course of the blood vessel changing and verified the fact that the second increase in blood flow is the result of flow dilation mediation. The effects of dilation of blood vessel were also analyzed.

1. Introduction

Hyperthermia is a traditional therapeutic procedure of heat application to certain points or areas on the surface of the body for disease treatment (Kumar and Rai, 2016). Skin blood flow increase and vasodilation are the two reactions in response to thermal stress (Khanafer et al., 2007). There have been numerous studies on heat-induced changes in blood flows in animal tumors (Reinhold and Endrich, 1986; Song, 1984) and in cutaneous tissue (Allwood and Burry, 1954; Nagasaka et al., 1987; Wu et al., 2017).

From the literitures (Kellogg et al., 1999; Minson et al., 2001; Widmer et al., 2006), local skin heating causes increases in cutaneous perfusion characterized by two distinct phases: (1) Within the first few minutes after the local application of heat, skin blood flow (SKBF) reaches a peak and then begins to decline; (2)Three to 5 min after heating, SKBF increases once again. Several studies have examined the mechanisms for the two phases of SKBF to local heating by drug blockade (Widmer et al., 2006). When a local anesthetic is used to block sensory input, the first phase of the biphasic flow response is abolished, suggesting sensory neural-mediated microvascular dilation. The second phase is diminished with the addition of nitric oxide (NO) synthase (NOS) inhibitors (Kellogg et al., 1999; Minson et al., 2001; Charkoudian, 2003), suggesting NO-dependent microvascular dilation.

A direct link between the mechanisms of the neural- and NO-mediated increases in flow has not yet to be established; however, shear stress has been postulated to play a role in the biphasic vasodilatory response (Kellogg et al., 1999; Minson et al., 2001; Widmer et al., 2006). Both experimental studies on vitro cell cultures and animal models, as well as, mathematical simulations have observed and predicted that increasing the wall shear stress on the endothelium can increase the production rate of NO (Buga et al., 1991; Garvin et al., 2010; Martini et al., 2006; Martini et al., 2005; Sriram et al., 2010; P.Ulker et al., 2011; Zhou a et al., 2012).

The endothelial cells that are covering the lumens of the arterial vessel can react to the wall shear stress variation induced by the increasing of blood flow during local heat. The physiological mechanism of vasodilation has been well studied. The wall shear stress variation triggers a complex cascade of regulation mechanism of blood vessel which involves the mass transfer and molecular diffusion of several materials. As a result, the vasodilatation occurs due to the relax of smooth muscles in the vessel wall. This is so called flow mediated dilation. Yamazaki proposed a mathematical model of flow mediated vasomotor response (Yamazaki and Kamiyama, 2014). Kudryashov (Kudryashov and Chernyavskii, 2008) established the flow mediated model to simulate the vessel response including the mass transfer of the key agents in the vessel wall and thus induced mechanical reflection of

* Corresponding author.
E-mail address: wang_yabo@tjcu.edu.cn (Y. Wang).

https://doi.org/10.1016/j.jtherbio.2019.07.022
Received 24 January 2019; Received in revised form 22 July 2019; Accepted 22 July 2019
Available online 23 July 2019

the vessel.

Using this information as a background, we hypothesized that there are at least two independent mechanisms contributing to the rise in SKBF during a local heating protocol. Therefore, our goal in the present study was to examine the interaction between neutrally and NO-mediated regulation of vascular response during local heating by mathematical method. According to previous researches, we hypothesized that the mechanism behind the blood flow increasing and vasodilatation were causally linked by FMD response. The dynamic blood flow was introduced into Kudryashov's autoregulation model to study the relationship between skin blood flow temperature and vasodilatation during heating. Investigating simultaneous inner mechanism of SKBF regulation during local heating can be beneficial in understanding and evaluating the potential efficacy and safety of hyperthermia treatment.

2. Experimental measurement

2.1. Materials and methods

The experiments were designed to test vasodilatation and variation in skin blood flow during the process of heating. The experimental system comprised two sections: the temperature controlling system and data acquisition system. The temperature controlling system consisted of a thermostatic water bath, a pump and a copper object stage. During the experiment, water at a predetermined temperature was pumped into the copper box to maintain constant temperature. After error analysis, the deviation does not exceed 0.1 °C. The data acquisition system included thermocouples, and a microscope as shown in Fig. 1.

The dorsal skin of a naked mouse was visualized using an intravital microscope and the image was relayed via camera to both a DVD player and a computer. To ensure uniform contact with object stage, the mouse was anaesthetized (by muscle injection with 2% chloral hydrate mixed with 10% urethane), and a part of its dorsal skin was cut by surgery and unfolded. The mouse was placed in a lateral position for the dorsal skin to be heated uniformly. The temperature of the object stage was set at 41, 43, and 45 °C. A roll on deodorant was smeared on the suscutis of the mouse to prevent the sweating. Thermocouples were placed on the object stage and the surface of the exposed suscutis. Studies were performed in a quiet room at 26 ± 2 °C. Images were recorded using a 1024 × 1024 camera focused on the specimen surface and linked to a computer for data acquisition. The images were taken during heating and post-processing.

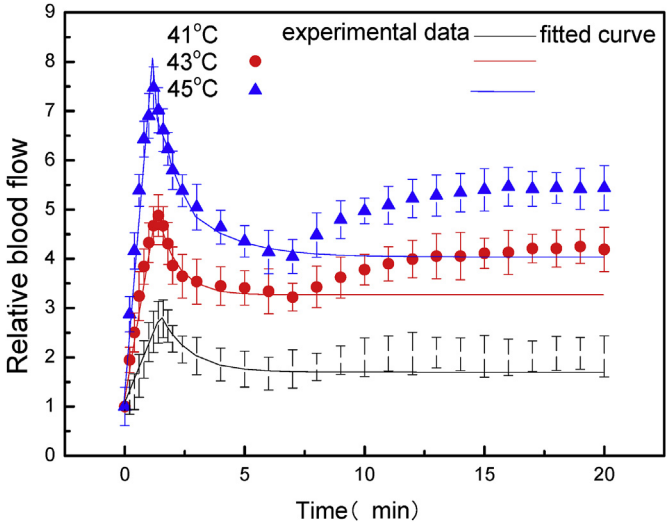

Fig. 2. Blood flow rate at different heating temperature.

2.2. Experimental results

Heating at 41, 43 and 45 °C induced dynamic changes in blood flow. The scatter points in Fig. 2 shows typical changes in skin blood flow upon heating at 41, 43 and 45 °C. The blood flow under normothermic conditions was set as the basic blood flow. As the skin surface temperature increased, the blood flow increased markedly and rapidly to a few multiples of its preheating value. This was followed by a transient drop and a secondary progressive rise to a plateau. These results are similar to those obtained in previous studied by Kellogg and Minson (Kellogg et al., 1999; Minson et al., 2001).

3. Mathematical model of blood vessel autoregulation

3.1. Description of FMD response model

Kudryashov's autoregulation model (Kudryashov and Chernyavskii,

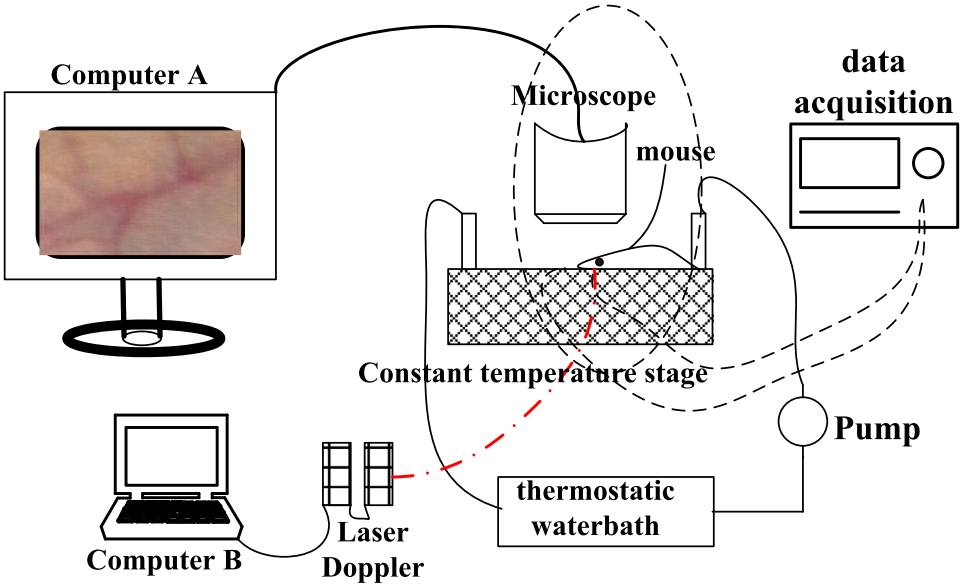

Fig. 1. Heating experimental system of rat skin.

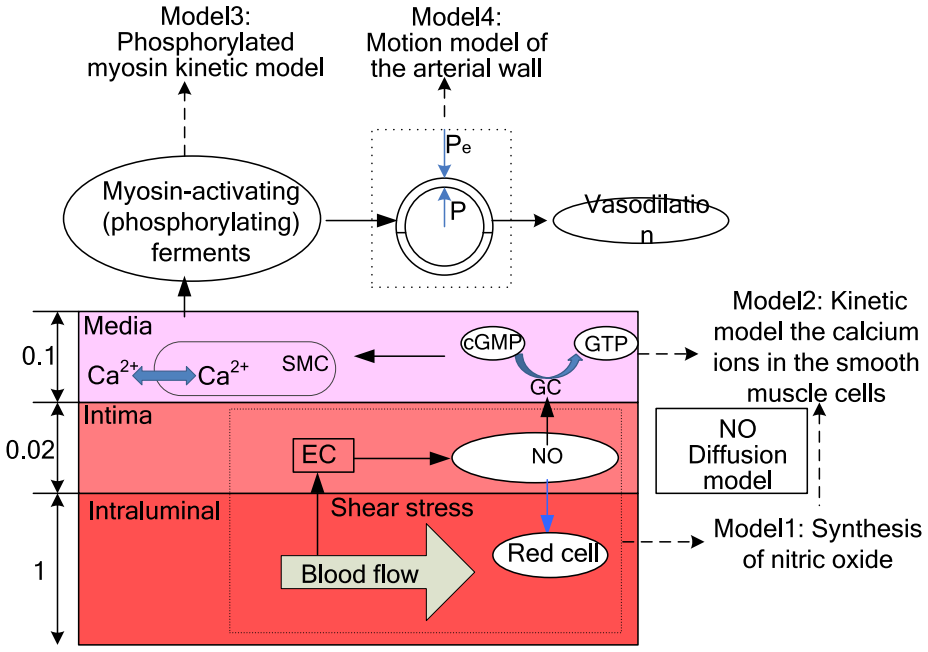

Fig. 3. Schematic of FDM regulation.

2008) was used by introducing the blood flow variation function which was the result of nerve regulation after heating. To maintain the integrity of present paper, we described only the important models in this paper. The autoregulation of the blood vessel takes place in an axially symmetric and viscoelastic tube. The vessel wall is treated as double layer structure. The intima(i) layer is lined with a single endothelia cell layer and the media (m) layer contains a single smooth muscle cell layer. The ratio of the thickness of the intraluminar: intima: media layer is 1:0.02:0.1. Four separate models were integrated to represent the FMD response. Fig. 3 shows the models and a schematic of their integration.

(1) Model 1: Synthesis and diffusion of NO

First, the wall shear stress stimulates the endothelial cell, and endogenous NO is synthesized. The NO concentration is computed according to the following differential equation:

$$\frac{dn_e}{dt} = -k_e n_e + k_3 \tau_{sh}(t) \tag{1}$$

where n_e is the NO concentration in the endothelial cell, τ is the wall shear stress, k_e is a coefficient characterizing mass transfer of NO from the endothelial cell into blood where NO is consumed by red cells, and k_3 is the endogenous NO production rate base on the wall shear stress. Considering the Hagen-Poiseuille profile of axial velocity, the relationship between blood flow rate and shear stress τ_{sh} is shown in Eq (2) (Tang and He, 2017).

$$\tau_{sh}(t) = -\mu \frac{\partial v_x(r)}{\partial r}\bigg|_{r=R(t)} = \frac{4\mu Q}{\pi R(t)^3} \tag{2}$$

where $R(t)$ is the inner radius of the artery, $\mu$is the dynamic viscosity of blood, and Q is the flow rate of blood. The diffusion and consumption of NO following its synthesis can be described as follows:

$$\frac{\partial n_j}{\partial t} = D_j \frac{1}{r}\frac{\partial}{\partial r}\left(r\frac{\partial n_j}{\partial r}\right) - \delta_j n_j \tag{3}$$

where n_j represents the concentration of NO and $j = 1,2$ denotes the inner layer and middle layer, respectively, of the arterial vessel. The first part of the equation on the right is the diffusion term and the second part represents the reaction along the arterial wall. D_j is the diffusion coefficient and δ_j is the reaction coefficient.

(2) Model 2: Kinetic model of the Ca^{2+} in smooth muscle cells; The NO synthesized rapidly diffuses into the neighboring vascular smooth muscle, where it activates soluble guanylate cyclase (sGC). This activation triggers on the conversion of guanosine triphosphate (GTP) into cyclicguanosine monophosphate (cGMP), which stimulates the outflow of intracellular calcium ions (Ca^{2+}). The remaining of Ca^{2+} in the smooth muscle cell layer corresponding to a coordinate r can be described by the following relationship:

$$\frac{\partial C(r,t)}{\partial t} = -(\alpha_1 + k_1 n_2)C + \phi_0 \tag{4}$$

where the first terms are represents for the active transportion of Ca^{2+} ions from the intracellular space and the second describes the inflow of Ca^{2+} ions from exterior to the interior of the smooth muscle cells, $\varphi_0 = \beta C_e = const$. The NO concentration in the media layer (n_2) calculated using Model 1 was used as the input to Kinetic model of the Ca^{2+} ions in the smooth muscle cells.

(3) Model 3: Phosphorylated myosin kinetic model

The stress developed by the smooth muscle cell depends on the intracellular concentration of Ca^{2+} ions and the Ca^{2+} sensitivity threshold of the specific myosin-activating (phosphorylating) ferments. The kinetics of phosphorylated myosin are described in the same way as the Ca^{2+} ion kinetics:

$$\frac{\partial f}{\partial t} = -a_2 f + r(C - C_{th})\theta(C - C_{th}) \tag{5}$$

where the first term is represents for the process of myosin dephosphorylation (deactivation) and the second describes the Ca^{2+}-dependent activation of the actin-myosin complex while accounting for the threshold of sensitivity to the Ca^{2+}concentration.θ is the Heaviside unit function, $\alpha_2$and $\gamma$are the phosphorylation and dephosphorylation rate coefficients, and C_{th} is the threshold concentration of Ca^{2+}.

(4) Model 4: Motion model of the arterial wall

In this model, the vessel wall is represented by its viscoelasticity and

active stress generated by the vascular smooth muscle (Carlson and Beard, 2011; Kapela and Tsoukias, 2011; Koenigsberger et al., 2006). According to the mechanical analysis on the arterial wall, the corresponding equation of motion for a segment of arterial wall can be obtained. The detailed description of Model 4 is provided in a previous study (Zhou a et al., 2012).

$$\rho_w h_0 R_0 \frac{d^2\eta}{dt^2} + \lambda h_0 \frac{d\eta}{dt} + k(F)[\eta + k_1\eta^2] = P_0 - \frac{h_0 k_2}{R_0} F \tag{6}$$

where$\eta = \frac{R-R_0}{R_0}$represents the radius perturbation, $P_0 = P - P_e$ is the difference between the internal and external pressures, and λ and h_0 are the nonlinear-elasticity and viscosity coefficients, respectively, of the arterial wall. $F = f(r, t)$is the concentration of the contracting actin-myosin filaments averaged over the smooth muscle layer volume, which determines the active muscular stress, k_1 is the nonlinear elastic coefficient, and k_2 is the coefficient of proportionality of the muscular tonus response to phosphorylated myosin concentration.

The dimensionless variables were introduced to the system of Eqs (1)–(6). The dimensionless variables are listed as follows:

$$n_e' = n_e/n^0,\ n_1' = n_1/n^0,\ n_2' = n_2/n^0$$

$$C' = C/C_{th},\ f' = f/F_0$$

$$t' = t/t_0,\ r' = r/R_0$$

The system of the equations changed to:

$$\frac{dn_e}{dt'} = -k_e' n_e' + \frac{\Psi'}{(1+\eta)^3} \tag{7}$$

$$\frac{\partial n_i'}{\partial t'} = D_i' \frac{1}{r'} \frac{\partial}{\partial r'}\left(r \frac{\partial n_i'}{\partial r}\right) - \delta_i' n_i' \tag{8}$$

$$i = 11 < r' < R_m',\ i = 2R_m' < r' < R_a'$$

$$\frac{\partial C(r', t')}{\partial t'} = -\alpha_1' C' - k_1' n_2' C' + \phi_0' \tag{9}$$

$$\frac{\partial f'}{\partial t'} = -\alpha_2' f' + \gamma'(C'-1)\theta(C'-1) R_m' < r < R_a' \tag{10}$$

$$\frac{d\eta}{dt'} + \lambda' \frac{d\eta}{dt'} + k_0'(1+\varepsilon F')[\eta + k_1'\eta^2] = P_0' - k_2' F,$$

$$F = \frac{2}{R_a'^2 - R_m'^2} \int_{R_m'}^{R_a'} f r dr \tag{11}$$

where the characteristic parameter n^0, C_{th}, F_0, t_0 and $R_0$are all constant number; $\Psi' = 4k_1\mu Q t_0/n^0(\pi R_0^3)$ in Eq. (7) and can represent dimensionless blood flow. The value of 10, as calculated by Lancaster (1994) was inputted as the basic flow rate. The coefficients in the equations should also be nondimensionalized. The values and process of nondimensionalization can be found in a reference (Kudryashov and Chernyavskii, 2008). The dimensionless coefficients are listed in Table 1 in this paper.

Table 1
Parameters calculated.

Parameters	Value	Source	Parameters	Value	source
k_e'	10	Kudryashov and Chernyavskii (2008)	α_2'	0.5	Kudryashov and Chernyavskii (2008)
Ψ_0'	10	Kudryashov and Chernyavskii (2008)	k_1'	0.015	Kudryashov and Chernyavskii (2008)
$D'_{1,2}$	0.0083	Regirer and Nkh (2005)	γ'	38.4615	Kudryashov and Chernyavskii (2008)
$\delta'_{1,2}$	0.1	Regirer and Nkh (2005)	λ'	5.113×10^9	Kudryashov and Chernyavskii (2008)
α_1'	0.5	Kudryashov and Chernyavskii (2008)	k_0'	4.55×10^8	Kudryashov and Chernyavskii (2008)
k_2'	1.519×10^9	Kudryashov and Chernyavskii (2008)	P_0'	1.549×10^9	Kudryashov and Chernyavskii (2008)
ϕ_0'	0.581	Kudryashov and Chernyavskii (2008)	ε	0.1	Kudryashov and Chernyavskii (2008)

Table 2
Fitted curve of blood flow at different heating temperature.

Heating temperature	Fitted Curve	
41 °C	$\begin{cases}\phi=0.99+1.19t \\ \phi=1.65+4.23\exp(-0.84t)\end{cases}$	$t<1.6min$ $t\geq 1.6min$
43 °C	$\begin{cases}\phi=0.99+2.90t \\ \phi=3.22+9.15\exp(-1.21t)\end{cases}$	$t<1.6min$ $t\geq 1.6min$
45 °C	$\begin{cases}\phi=0.99+5.86t \\ \phi=3.99+6.26\exp(-0.51t)\end{cases}$	$t<1.6min$ $t\geq 1.6min$

3.2. Assumption and adaption of FMD model during heating

After nondimensionalization, the FMD model will be have universal applicability in predicting the behavior of blood vessels. Previous studies have shown that the initial increase in blood flow is mainly due to the role of nerve regulation, while the subsequent increase in blood flow is the result of vascular dilation under the role of FMD. In this paper, it is assumed that vasodilatation is the result of the initial increase in blood flow. Therefore, the second increase in blood flow is not considered when the curve of blood flow variation is being fitted. Based on the relative blood flow rates obtained from the experiments, a piecewise function is used to fit the curve. The linear function is used to fit the ascending region of blood flow, and the power exponential function is used to fit the declining and steady state region of the blood flow. The fitted results of the relative blood flow at different heating temperature are shown in Table 2.

4. Results

The fitted curve of blood flow was introduced as the multiple power of the basic blood flow to Eq. (2) in the simulation. The model equations given by Eqs. (7)-(11) are coupled and must be solved simultaneously. This system of equations was solved numerically by first using the dynamic blood flow rate. An implicit finite difference method was employed. In each time step, we carried out iterations in the Ca^{2+} concentration and applied the trapezoidal rule to determine the radius deviation. A uniform grid with a radial step $\Delta r' = 1.2 \times 10^{-3}$, time step $\Delta t = 1.2 \times 10^{-3}$and iteration error of 1×10^{-4} was used.

4.1. Concentration of key agents participated in autoregulation

It can be seen from Fig. 2 that when the local heat temperature was increased to 41 °C, the result was a rapid increase in skin blood flow to an initial peak value. This was followed by a chain of FMD reaction as shown in Fig. 4. The increased blood flow accelerated the production of NO and consumption of Ca^{2+} and *f*. Therefore, the blood vessel diameter increased to a high level.

Autoregulation occurs in response to changes in blood flow rate; it is a result of the damping of oscillations and finally reaches a new equilibrium state. There exists an initial peak for each reactive agent. It took 3.4min, 19.2min, and 22.2min for NO, Ca^{2+}, *f*, respectively, to reach their peak values. From Fig. 4, it can be seen that it took nearly 50 min

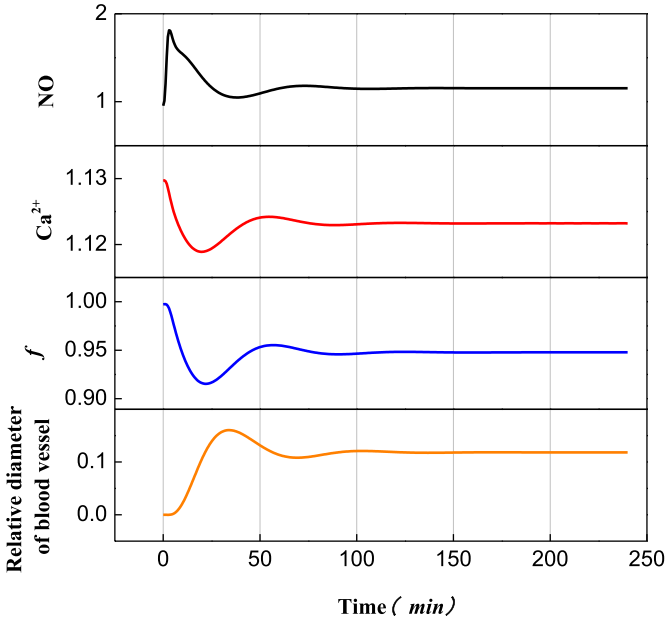

Fig. 4. A sequence of reactions of shear stress regulation response at the local temperature of 41 °C.

for the blood vessel diameter to reach a steady value. Zhang's experimental data led to a similar conclusion (Zhang, 2003).

Fig. 5A shows the variation in NO concentration with time and diameter. The initial distribution of NO concentration was obtained when at a blood flow rate of 1. Shear stress increased upon heating owing to the increasing in blood flow. The endothelial cell located at the intima layer of the vessel wall first responded to the variation in the shear stress and accelerated NO synthesis. Although, the red cells consume some of the NO, the concentration of the NO in the intima layer was maintained at a high level because the sole source of NO is its production in the endothelial cells. At the beginning of autoregulation, the NO concentration decreased sharply along the vessel wall. It then decreased near intima layer and increased along the vascular smooth muscle, and finally, tended to a new equilibrium state (purple curve) gradually, as shown in Fig. 5A.

The variations in the concentrations of Ca^{2+} and f took place in the smooth muscle cells, which compose the media membrane of the blood vessel. Thus, the starting position for the concentrations of calcium ion and phosphorylated myosin is 1.02. The concentration of Ca^{2+} increased slightly in the radial direction, as shown in Fig. 5B. Since the Ca^{2+} concentration was above the sensitivity threshold ($C_{th} = 1$), the Ca^{2+} concentration-dependent myosin phosphorylation was in an active state. Therefore, the concentration of phosphorylated myosin along the radial direction also increased with Ca^{2+} concentration as shown in Fig. 5C.

4.2. Process of autoregulation at different heating temperature

Different heating temperatures have different effects on blood flow and vessel diameter. Fig. 6 shows the variation in the concentration of NO, Ca^{2+} and dephosphorylation myosin at the interface of the intima and media layers. Higher temperature leads to increased reaction rate and higher NO concentration. The oscillation attenuation also presents a higher rate and higher degree at higher heating temperature. Similar trends in concentration variation can be obtained in the case Ca^{2+} ions and dephosphorylation myosin but the direction of variation are opposite to that of NO. The concentration of NO displays drastic changes when compared with those of Ca^{2+} and dephosphorylation myosin. The maximum change occurred at 45 °C when the NO concentration increased to 4.4 times its initial value. However, the degree of variation in

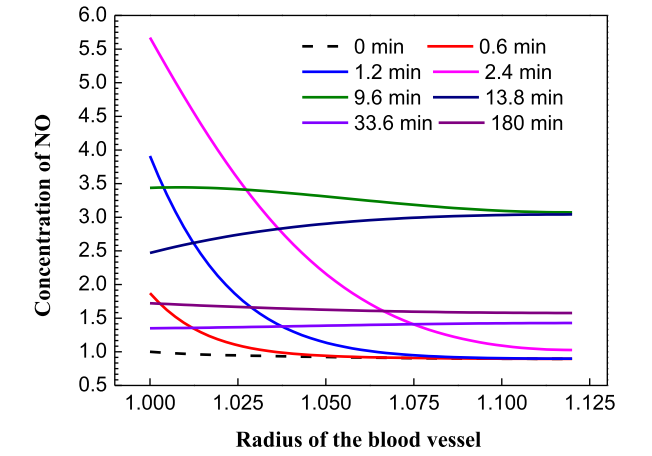

(A) Concentration variation of NO at different locations and time

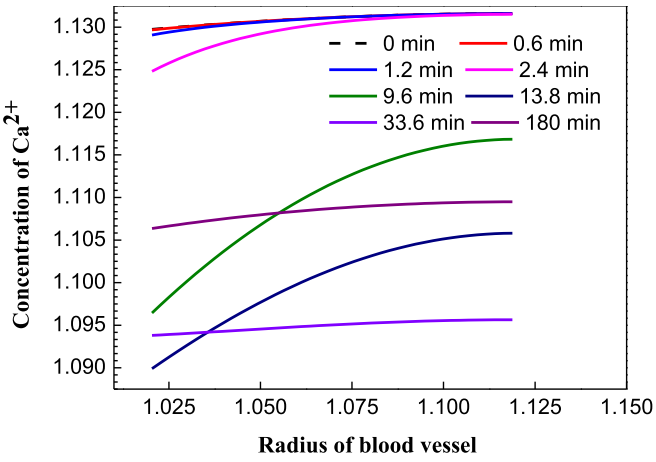

(**B**) Concentration variation of Ca^{2+} at different locations and time

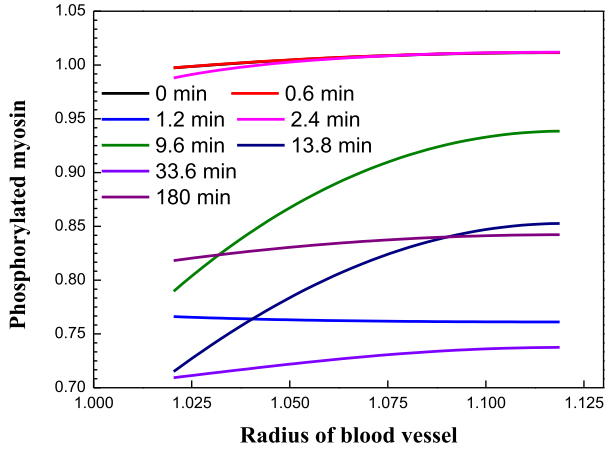

(**C**) Concentration variation of phosphorylated myosin at different locations and time

Fig. 5. Concentration distributions in the vessel wall: NO, intracellular Ca^{2+}, phosphorylated myosin (A) Concentration variation of NO at different locations and time. (**B**) Concentration variation of Ca^{2+} at different locations and time (**C**) Concentration variation of phosphorylated myosin at different locations and time.

Ca^{2+} concentration was in range 1.09–1.13 and that of f is ranged from 0.7–1.0.

Fig. 6D shows the variation in diameter during heating. Oscillation attenuation occurred in vessel diameters. However, the amplitude of regulation declined to a very low value after one cycle. Therefore, a

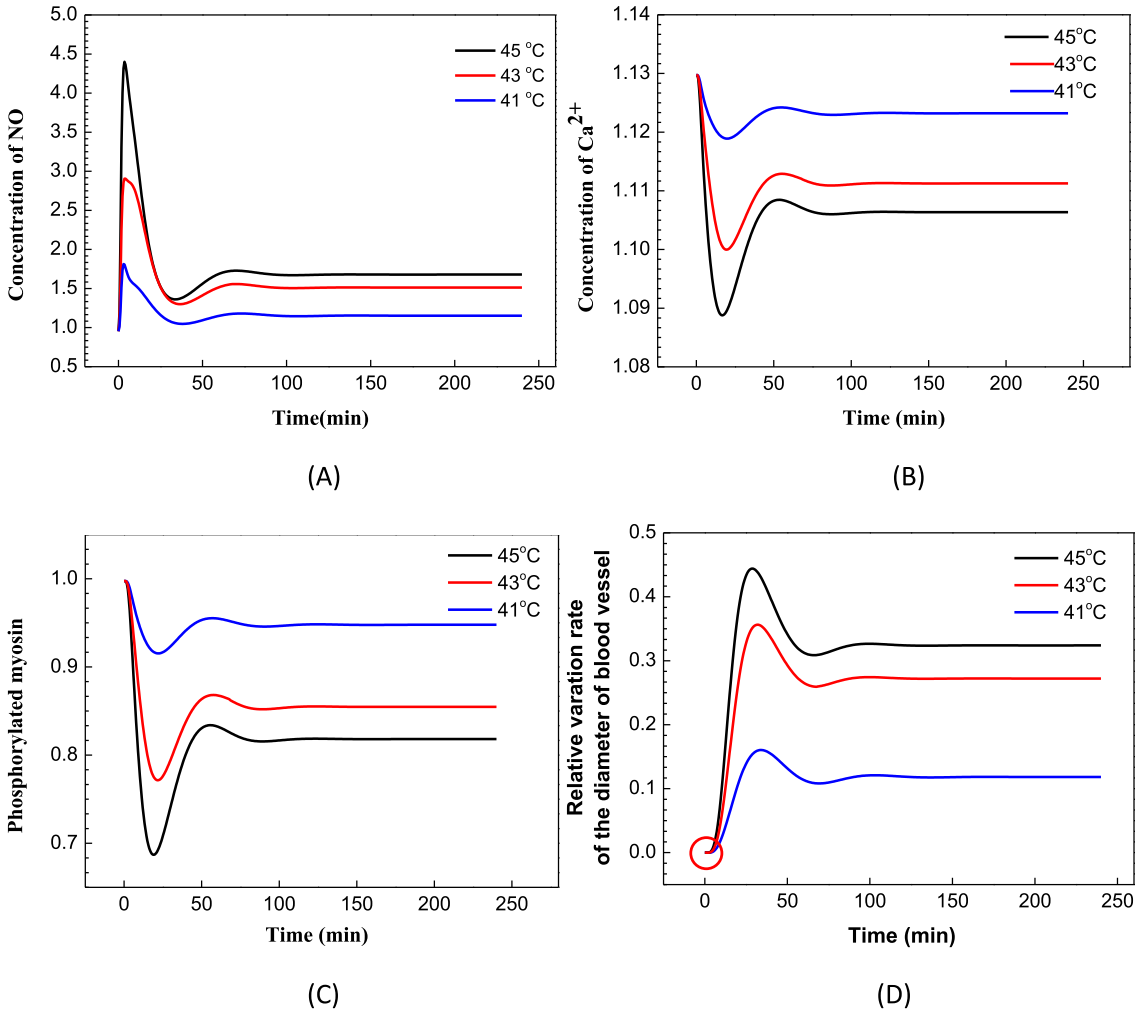

Fig. 6. Time dependence of the relative change in the concentration of NO (A), Ca^{2+} (B), phosphorylated myosin (C)and vessel radius (D)during regulation response at different heating.

rapid increase followed by a transient drop in vessel diameter, and a subsequent, small secondary progressive rise to a plateau can be seen. Higher heating temperatures led to significantly greater dilation whereas the vessels dilated to a significantly lower degree at lower heating temperature. The final rates of variation in vessel diameter are 0.12, 0.27 and 0.32.

5. Discussions

5.1. Flow resistance and second increase in blood flow

Flow resistance is a parameter independent of flow rate and pressure difference. It depends on viscosity, length and diameter. According to the definition of the flow resistance [28], an increase in vessel diameter can reduce flow resistance, as shown in Eq. (12).

$$R_f = \frac{8\mu L}{\pi R^4} \tag{12}$$

Fig. 7 shows the relative change in flow resistance caused by vasodilation under heating at different temperatures. Higher heating temperature led to lower flow resistance which thereby promoting blood flow. The reaction time is defined as the period from the beginning of heating to vessel dilation, which is marked in the circle in Fig. 6D. The exact times are illustrated in Fig. 7. It takes approximately 3–5 min for the blood vessel to dilate, which verifies the fact that the second increase in blood flow is the result of FDM.

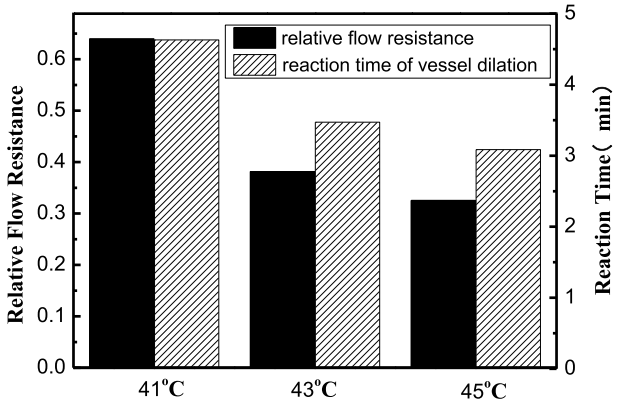

Fig. 7. Flow resistance and reflection time of vascular changes at different temperatures.

5.2. Effect of keeping constant wall shear stress

According to Eq. (1), the FMD response can cause a change in the vascular circumferential wall stress. For the blood vessel to remain unchanged when heated, the vascular wall should endure greater wall shear stress. Fig. 8 shows a comparison between the wall shear stresses of constant and enlarged vessel wall. Higher heating temperature resulted in greater increase in the blood flow and vessel diameter. The

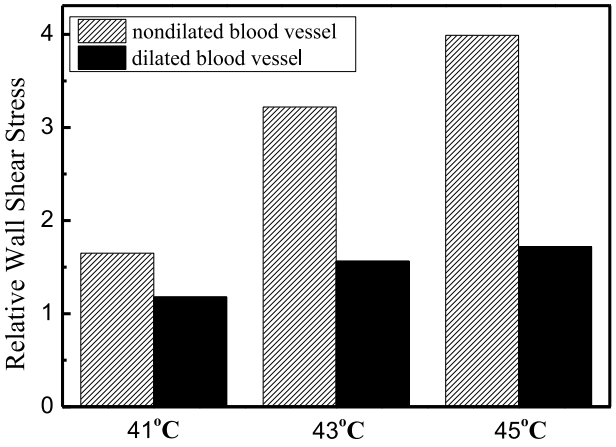

Fig. 8. Comparison of wall shear stress between dilated vessel and nondilated vessel.

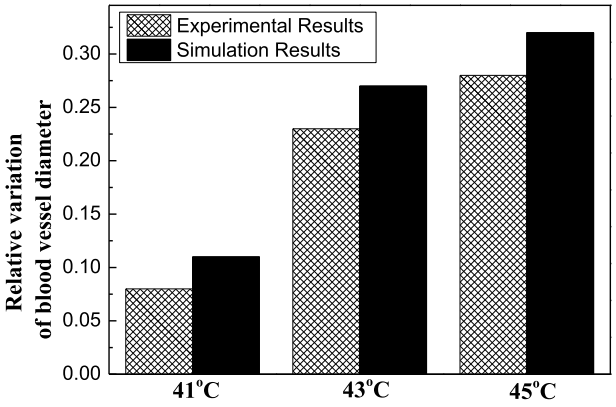

Fig. 9. Comparison of the experimental and numerical dependences of the change in artery diameter.

increase in vascular diameter largely limits the increase in wall shear stress, which is very important for maintaining the relative stability of vascular endothelial stress. This physiological behavior effectively reduces cell inflammation and apoptosis caused by excessive wall shear stress on blood vessels [29,30].

5.3. Limitations of present model

In Fig. 9, the relative diameter obtained by experiments and numerical simulations are compared, and a few difference are observed. The calculated value of diameter is much higher than the experimental value. This is due to the effect of other mechanism of regulation such as: (a) myogenic response of arterioles, capillaries and microcirculation venules; and (c) neural and metabolic control [31]. Myogenic response was considered as a function of intravascular pressure in most studies. Any shear-dependent vasodilatation results in an increase in wall tension and generates vasoconstriction due to myogenic response. Thus, this model may overestimate the vasodilatation response. However, previous studies have established that the rapid reflection of blood flow during heating is controlled by neural and metabolic mechanism. The shear-dependent response is the main mechanism next to neural regulation of blood flow.

Molecular dynamic behavior in cells will be different at different temperature. However, ignoring the temperature effects in the molecular dynamic is another factor affecting the accuracy of this model. This kind of investigation will be very interesting and attract of our attention in the future.

6. Summary

A numerical study was conducted to determine the effect of temperature on blood flow and vessel diameter in skin. The experiment established the dorsal skin of the naked mouse as a model for studying intact, thermoregulatory microvascular beds and obtained the law of the blood flow variation. The behavior of vasodilatation during heating was predicted by using the flow mediated model considering dynamic blood flow, in which variations in concentrations of key agents during autoregulation were additionally determined. Based on mathematical analysis, it was proved that the effect of vasodilatation can maintain vessel stress balance. Moreover, we provided evidence that FMD can lead to a second increase in blood flow. The model parameters are related to blood flow and vessel diameter and can be used to aid in accurate temperature prediction in the treatment of hyperthermia.

Acknowledgments

This work was supported by the National Natural Science Foundation of China (No.51506151) and the Natural Science Foundation of Tianjin (NO.16JCQNJC14000).

References

Allwood, M.J., Burry, H.S., 1954. The effect of local temperature on blood flow in the human foot. J. Physiol. 124, 345–347.
Buga, G.M., Gold, M.E., Fukuto, J.M., Ignarro, L.J., 1991. Shear stress-induced release of nitric oxide from endothelial cells grown on beads. Hypertension 17 (2), 187–193.
Carlson, B.E., Beard, D.A., 2011. Mechanical control of cation channels in the myogenic response. Am. J. Physiol. Heart Circ. Physiol. 301 (2), 331–343.
Charkoudian, N., 2003. Skin blood flow in adult human thermoregulation: how it works, when it does not, and why. Mayo Clin. Proc. 78 (5), 603–615.
Garvin, J.L., Cabral, P.D., Hong, N.J., 2010. Shear stress increases nitric oxide production in thick ascending limbs. Am. J. Physiol Renal. 299 (5), 1185–1192.
Kapela, A., Tsoukias, N.M., 2011. Multiscale FEM modeling of vascular tone: from membranecurrents to vessel mechanics. IEEE Trans. Biomed. Eng. 58 (12), 3456–3459.
Kellogg, D.L., Liu, Y., Kosiba, I.F., O'Donnell, D., 1999. Role of nitric oxide in the vascular effects of local warming of the skin in humans. J. Appl. Physiol. 86 (4), 1185–1190.
Khanafer, K., Bull, J.L., Pop, I., Berguer, R., 2007. Influence of pulsatile blood flow and heating scheme on the temperature distribution during hyperthermia treatment. Int. J. Heat Mass Transf. 50 (23), 4883–4890.
Koenigsberger, M., Sauser, R., Beny, J., Meister, J., 2006. Effects of arterial wall stress on vasomotion. Biophys. J. 91 (5), 1663–1674.
Kudryashov, N.A., Chernyavskii, I.L., 2008. Numerical simulation of the process of autoregulation of the arterial blood flow. Fluid Dyn. 43 (1), 32–48.
Kumar, D., Rai, K.N., 2016. A study on thermal damage during hyperthermiatreatment based on DPL model for multilayer tissues using finite element Legendre wavelet Galerkinapproach. J. Therm. Biol. 62, 170–180.
Lancaster, J.R., 1994. Simulation of the diffusion and reaction of endogeneouslyproduced nitric oxide. Proc. Natl. Acad. Sci. USA 91 (17), 8137–8141.
Martini, J., Carpentier, B., Negrete, A.C., Frangos, J.A., Intaglietta, M., 2005. Paradoxical hypotension following increased hematocrit and blood viscosity. Am. J. Physiol. Heart Circ. Physiol. 289 (5), 2136–2143.
Martini, J., Carpentier, B., Negrete, A.C., Cabrales, P., Tsai, A.G., Intaglietta, M., 2006. Beneficial effects due to increasing blood and plasma viscosity. Clin. Hemorheol. Microcirc. 35 (1–2), 51–57.
Minson, C.T., Berry, L.T., Joyner, M.J., 2001. Nitric oxide and neurally mediated regulation of skin blood flow during local heating. J. Appl. Physiol. 91 (4), 1619–1626.
Nagasaka, T., Hirata, K., Nunomura, T., Cabanac, M., 1987. The effect of local heating on blood flow in the finger and the forearm skin. Can. J. Physiol. Pharmacol. 65 (6), 1329–1332.
Ulker, P., Yaras, N., Yalcin, O., Celik-Ozenci, C., Johnson, P.C., Meiselman, H.J., Baskurt, O.K., 2011. Shear stress activation of nitric oxide synthase and increased nitric oxide levels in human red blood cells. Nitric Oxide 24 (4), 184–191.
Regirer, S.A., Nkh, S., 2005. Mathematical models of nitric oxide transportin a blood vessel. Biofizika 50 (3), 515–536.
Reinhold, H.S., Endrich, B., 1986. Tumor microcirculation as a target for hyperthermia. Int. J. Hyperth. 2 (2), 111–137.
Song, C.W., 1984. Effect of local hyperthermia on blood flow and microenvironment: a review. Cancer Res. 44 (10), 472l–4730.
Sriram, K., Vazquez, B.Y., Yalcin, O., Johnson, P.C., Intaglietta, M., Tartakovsky, D.M., 2010. The effect of small changes in hematocrit on nitric oxide transport in arterioles. Antioxidants Redox Signal. 14 (2), 175–185.
Tang, Y., He, Y., 2017. Model analysis of Endothelium-dependent vasomotion of small artery. Chin. J. Theor. Appl. Mech. 49 (1), 182–190.
Widmer, R.J., Laurinec, J.E., Young, M.F., Laine, G.A., Quick, C.M., 2006. Local heat produces a shear-mediated biphasic response in the thermoregulatory

microcirculation of the Pallid bat wing. Am. J. Physiol. Regul. Integr. Comp. Physiol. 291 (3), 625–632.
Wu, Y., Nieuwenhoff, M.D., Huygen, F.J.P.M., van der Helm, F.C.T., Niehof, S., Schouten, A.C., 2017. Characterizing human skin blood flow regulation in response to different local skin temperature perturbations. Microvasc. Res. 111, 96–102.
Yamazaki, Y., Kamiyama, Y., 2014. Mathematical model of wall shear stress-dependent vasomotor, response based on physiological mechanisms. Comput. Biol. Med. 45 (1), 126–135.
Zhang, Ting, 2003. Dynamic Study of Blood Flow Changes during Local Hyperthermia. MS Thesis. Huazhong University of Science and Technology, Wuhan, China.
Zhou a, Y., Cabrales, P., Palmer, A.F., 2012. Simulation of NO and O_2 transport facilitated by polymerized hemoglobin solutions in an arteriole that takes into account wall shear stress-induced NO production. Biophys. Chem. 162, 45–60.